

Harmonizing the Deep: A Unified Information Pipeline for Robust Marine Biodiversity Assessment Across Heterogeneous Domains

Marco Piccolo¹, Qiwei Han², Astrid van Toor³, Joachim Vanneste⁴,

^{1,2}Nova School of Business & Economics, Carcavelos Portugal

^{3,4}blueOASIS, Ericeira, Portugal

{63996, qwei.han} @novasbe.pt, {avtoor, jvanneste}@blueoasis.pt,

Abstract

Marine biodiversity monitoring requires scalability and reliability across complex underwater environments to support conservation and invasive-species management. Yet existing detection solutions often exhibit a pronounced deployment gap, with performance degrading sharply when transferred to new sites. This work establishes the foundational detection layer for a multi-year invasive species monitoring initiative targeting Arctic and Atlantic marine ecosystems. We address this challenge by developing a Unified Information Pipeline that standardises heterogeneous datasets into a comparable information flow and evaluates a fixed, deployment-relevant detector under controlled cross-domain protocols. Across multiple domains, we find that *structural* factors, such as scene composition, object density, and contextual redundancy, explain cross-domain performance loss more strongly than *visual* degradation such as turbidity, with sparse scenes inducing a characteristic “*Context Collapse*” failure mode. We further validate operational feasibility by benchmarking inference on low-cost edge hardware, showing that runtime optimisation enables practical sampling rates for remote monitoring. The results shift emphasis from image enhancement toward structure-aware reliability, providing a democratised tool for consistent marine ecosystem assessment.

1 Introduction

Marine ecosystem monitoring provides essential evidence for understanding ocean health and supporting timely management responses to environmental change [Mieszkowska *et al.*, 2014]. Climate-driven shifts in species distributions, habitat fragmentation, and rising pressure from biological invasions threaten marine sustainability and accelerate biodiversity loss [European Commission *et al.*, 2013]. In Europe, invasive species affect a substantial share of threatened taxa and continue to pose persistent risks to marine and coastal ecosystems [European Commission, 2020; National Oceanic and Atmospheric Administration, 2025]. These challenges align directly with UN Sustainable Development Goal 14 (Life Be-

low Water) [United Nations, 2015] and the EU Biodiversity Strategy for 2030 [European Commission, 2020], motivating scalable, field-deployable tools that can monitor biodiversity consistently across space and time.

Conventional monitoring approaches remain costly and difficult to scale. Fisheries surveys sample only portions of populations and face accuracy and logistics constraints [Labrosse *et al.*, 2002]. Manual visual census depends on human judgement and introduces observer bias, while environmental DNA (eDNA) requires repeated physical sampling to track diversity and abundance [Rourke *et al.*, 2022; Ruppert *et al.*, 2019]. These limitations have accelerated interest in non-destructive automated monitoring [McGeady *et al.*, 2023]. In terrestrial settings, deep learning can replace time-intensive manual surveys while producing competitive population estimates [Torney *et al.*, 2019]. In underwater settings, automated fish detection can outperform experts and citizen scientists on curated benchmarks [Ditria *et al.*, 2020]. However, such results also highlight a deployment-relevant asymmetry: even when average accuracy is high, false negatives can remain elevated in operational streams, which is consequential for early-warning monitoring of rare or invasive individuals.

The central obstacle for marine deployment is therefore not achieving high accuracy on a single curated dataset, but ensuring that detection outputs remain *comparable and trustworthy across deployments* [Wang *et al.*, 2022]. In practice, models tuned for one site often degrade sharply when transferred to new habitats, camera viewpoints, or ecological contexts [Recht *et al.*, 2019]. This *deployment gap* forces practitioners to build ad hoc site-specific models without clear guidance on whether failures are driven primarily by visual degradation (turbidity, colour attenuation, blur) or by structural properties of the scene (object density, overlap/occlusion, contextual redundancy). For biodiversity monitoring, this distinction is operationally decisive: unstable sensitivity across sites can create spurious trends, while missed detections can suppress early warning signals.

We address this gap by reframing the underwater fish detection task [Elmezain *et al.*, 2025; González-Sabbagh and Robles-Kelly, 2023; Jian *et al.*, 2024; Xu *et al.*, 2023] as an *information reliability* problem: the goal is to produce detection outputs that remain interpretable as monitoring evidence under domain shift, subject to operational

constraints. The study is co-designed with two stakeholder roles: marine ecologists, who require cross-site comparability and recall-sensitive outputs for early warning, and technical operators, who impose compute, memory, and connectivity constraints that bound feasible deployment. We develop a unified information pipeline that standardises heterogeneous datasets into a comparable representation and evaluate a fixed, deployment-relevant detector under controlled cross-domain protocols. Holding the detector fixed isolates domain effects attributable to data and environment, enabling an auditable diagnosis of when and why reliability fails under transfer.

A key methodological point is that “scene structure” induces two qualitatively different failure regimes. In sparse, low-redundancy scenes, isolated targets provide few contextual cues for verification, leading to a recall collapse (“*Context Collapse*”) [Geirhos *et al.*, 2020]. In dense, high-overlap scenes, occlusion and silhouette merging reduce separability and shift errors toward missed detections and localization failures. This two-regime framing reconciles cases where increasing density improves recall (sparse-to-moderate transition) with cases where increasing density/overlap harms recall (moderate-to-crowded transition), and it supports monitoring-facing interpretation beyond standard detection metrics (mAP, precision, recall).

Our contributions are:

- **Unified reliability pipeline.** We design an end-to-end pipeline that harmonises cleaning, annotation, deduplication, and evaluation across heterogeneous underwater datasets, enabling controlled comparison of detector behaviour under monitoring-relevant constraints.
- **Controlled cross-domain diagnosis with covariate controls.** We introduce stress tests and image-level diagnostic covariates that separate visual degradation from scene structure, and we quantify their relative association with detection success using a mixed-effects attribution model that controls for dataset-level heterogeneity.
- **Mechanistic error characterization.** We complement aggregate metrics with a standard detection error decomposition (TIDE-style categories) to distinguish verification-driven misses in sparse regimes from separability-driven errors in crowded regimes [Bolya *et al.*, 2020].
- **Deployment feasibility evidence.** We validate operational feasibility via edge benchmarking on low-cost hardware (NVIDIA Jetson Nano), showing that hardware-aware optimisation (TensorRT) supports practical sampling rates for long-horizon monitoring deployments [Han *et al.*, 2016].

Reproducibility and artifacts. To support reproducibility and deployment-oriented reuse while preserving double-blind review, preprocessing scripts, metric computation code, training configurations, and benchmarking protocols are provided in anonymised supplementary material.

2 Stakeholder Co-Design and Operational Context

This work follows a bottom-up co-design approach grounded in the operational realities of long-horizon underwater monitoring, as the foundational detection layer for a multi-year

invasive species monitoring initiative targeting Arctic and Atlantic marine ecosystems. The study is informed by a multi-lateral collaboration between (i) technical operators responsible for autonomous sensing infrastructure, edge compute, and data pipelines, and (ii) marine ecologists who use derived indicators for biodiversity assessment and early-warning monitoring. To ensure the system targets deployment bottlenecks rather than abstract benchmarks, we elicited requirements through structured consultations with these stakeholder roles. These consultations directly shaped the evaluation priorities (cross-site comparability; recall-sensitive failure modes), bounded model choice by operational constraints (edge memory/latency), and defined the form of monitoring impact considered valid (comparability of indicators under domain shift rather than peak in-domain accuracy).

(R1) Ecologists: Cross-site comparability. Ecologists required that indicator trends remain comparable across sites, so that apparent changes are not artefacts of camera, viewpoint, habitat, or acquisition protocol. *Design response:* we standardise heterogeneous sources into a unified information pipeline (Section 3) and evaluate transfer under controlled stress tests that hold the detector fixed (Section 4.4), isolating domain effects from architectural confounds. *Validation evidence:* the Luderick stress test (Table 7) provides evidence that the fixed detector can retain usable performance under a habitat/appearance shift with relatively favourable visibility, supporting comparability claims within that operating regime.

(R2) Ecologists: False-negative asymmetry for early warning. For invasive or rare species monitoring, stakeholders prioritised avoiding missed detections over maximising aggregate accuracy. *Design response:* we treat recall (and recall-at-precision operating points) as a primary diagnostic and explicitly attribute false negatives to structural versus visual drivers under domain shift (Section 5.4). *Validation evidence:* the DeepFish stress test (Table 6) exhibits a pronounced recall degradation in a low-redundancy regime, consistent with a sparsity-driven “*Context Collapse*” failure mode that is operationally critical for early warning.

(R3) Operators: Edge feasibility under constrained memory, power, and connectivity. Operators required that the system run on 4GB-class edge nodes with limited power budgets and intermittent connectivity, making continuous uplink impractical. *Design response:* these constraints bound model selection and motivate hardware-aware export and acceleration (Section 4.3), evaluated on representative commodity hardware. *Validation evidence:* edge benchmarking demonstrates that TorchScript conversion can exceed a 4GB budget (OOM) while TensorRT enables practical sampling throughput (Table 8), establishing feasibility for long-horizon, low-rate monitoring policies.

(R4) Operators: Operational guardrails against spurious detections. Operators required guardrails against false alerts that inflate review workload and waste bandwidth in low-prevalence deployments. *Design response:* we retain background-only frames to preserve negative-class diversity and treat precision as an operational constraint rather than a secondary metric (Section 3, Section 5). *Validation evidence:*

Dataset	Environment	Description & key challenges (Structure / Visual)
OzFish [AIMS <i>et al.</i> , 2019]	Coastal BRUVS	High fish density and frequent overlap near bait (density/occlusion); variable illumination and backscatter (lighting/turbidity), with only 350 cleaned images retained from a larger BRUVS pool due to annotation errors.
DeepFish [Saleh <i>et al.</i> , 2020]	Tropical reefs	Sparse targets with low contextual redundancy (sparsity); strong blur and low contrast in turbid water (blur/contrast).
Luderick [Global Wetlands Project, 2020]	Seagrass beds	Dynamic vegetation and background motion (background dynamics); dominant green cast and visibility variation (colour cast/turbidity).
AquaCoop	Aquaculture cages	Monoculture (<i>D. labrax</i>) with net occlusion and overlapping silhouettes (occlusion/shape ambiguity); repetitive lighting patterns and specularities (illumination/reflections).
Fish4Knowledge [Fisher <i>et al.</i> , 2016]	Coral reefs	Complex backgrounds and frequent small instances (background clutter/scale); high turbidity and colour attenuation (turbidity/colour).
LifeCLEF [Joly <i>et al.</i> , 2015]	Tropical reefs	High biodiversity with multiple co-occurring species (multi-object scenes); mixed illumination and viewpoint changes (lighting/viewpoint).
Aquarium [Dwyer, 2022]	Controlled tanks	Lower background complexity with occasional glass artifacts (simple structure/reflections); artificial lighting and glare (illumination/specular).
Open Ocean [Roboflow, 2021]	Open ocean	Wide variation in scene composition and scale (structure variability); strong natural-light variation (illumination).

Table 1: Eight heterogeneous sources comprising the unified pipeline. The selection spans structural conditions (sparse vs. dense; low vs. high occlusion) and visual conditions (turbid vs. clear; colour cast), enabling controlled analysis of cross-domain reliability.

baseline precision on the selected fixed detector (Table 2) supports adherence to this guardrail and motivates its use in subsequent cross-domain analyses.

3 Unified Information Pipeline

We operationalise marine invasive species monitoring as an *information reliability pipeline*: heterogeneous raw imagery is transformed into a standardised representation that supports controlled model training, comparable evaluation, and diagnostic analysis of failure modes under domain shift. A schematic of the end-to-end pipeline (dataset harmonisation, training, cross-domain tests, and edge benchmarking) is provided in Appendix B.

3.1 Heterogeneous Underwater Image Sources

To support generalisation under long-term deployment variability, the pipeline integrates eight datasets summarised in Table 1. The sources span monitoring-relevant environments, from controlled aquaculture monocultures (AquaCoop) to complex, high-biodiversity reef scenes (e.g., Fish4Knowledge). They are selected to induce systematic variation along two axes: (i) *scene structure* (density, overlap/occlusion, background dynamics) and (ii) *visual quality* (turbidity/backscatter, blur/contrast, colour cast, illumination). This heterogeneity supports controlled cross-domain evaluation and enables diagnosis of whether reliability losses are primarily structural or visual. The integrated corpus contains 28,765 images and is split into 70% training (20,130), 20% validation (5,752), and 10% testing (2,883) with the same class distribution.

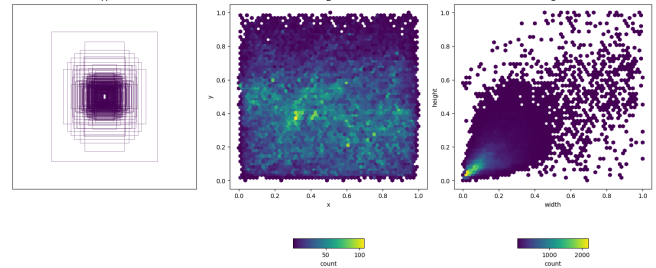


Figure 1: Unified annotation distribution. A) Spatial geometry of 300 sampled bounding boxes; B) Centroid density map; C) Width–height distribution illustrating variation in object size across datasets.

3.2 Annotation Standardisation and Harmonisation

A prerequisite for cross-domain comparability is a unified annotation representation. All datasets are converted into a YOLO-compatible format where each instance is represented as `class_id center_x center_y width height`, with all coordinates normalised to $[0, 1]$ to ensure consistent geometry across images with different resolutions and aspect ratios. For datasets using polygon masks or XML contour formats, polygons are converted to minimal enclosing rectangles prior to normalisation and export. Figure 1 summarises the unified annotation space, including sampled bounding boxes, centroid density, and width–height distributions.

3.3 Data Integrity, Deduplication, and Split Protocol

All images and labels undergo structured cleaning and validation prior to integration. To prevent leakage and reduce redundancy, we apply multi-stage deduplication: (i) path-level checks to resolve duplicate references, (ii) perceptual hashing (aHash) to detect near-duplicate frames, and (iii) MD5 hashing to detect exact duplicates. Hashes are computed for both images and label files; for each duplicate group, a single representative sample is retained.

To focus the study on detection reliability rather than taxonomy, all class labels are mapped to a single *fish* class. Images without valid labels after cleaning are retained as background-only samples to preserve negative-class diversity, reducing spurious detections in low-prevalence monitoring regimes.

The 70/20/10 split is constructed via a stratified two-step procedure. We first sample a held-out test set, then split the remaining data into training and validation. Stratification keys combine (a) source dataset identity and (b) presence/absence of fish annotations, ensuring balanced representation across datasets while preserving the positive/negative ratio in each subset.

3.4 Diagnostic Metrics: Visual Quality and Scene Structure

Even under stratified splitting, substantial domain differences remain. To disentangle whether performance failures are

driven primarily by visual degradation or by scene composition, we compute no-reference diagnostic metrics for every image and summarise them at the dataset level for descriptive analysis. These metrics are used only as covariates for interpretation, not for model optimisation.

Visual degradation metrics. We compute two established underwater image quality measures: UIQM [Panetta *et al.*, 2015] and UCIQE [Yang and Sowmya, 2015]. To complement these perceptual scores, we compute additional proxies: (i) a haze/backscatter proxy (“turbidity”) based on image statistics, (ii) RGB channel ratios to characterise colour cast, (iii) RMS contrast, and (iv) a Laplacian-variance blur proxy.

Scene structure metrics. To test whether structural composition explains cross-domain failures beyond image quality, we compute: (v) Object Density, the number of annotated fish per image; and (vi) Structural Overlap, defined per image as the mean (over ground-truth boxes) of the maximum pairwise Intersection-over-Union (IoU) with any other ground-truth box. These metrics capture sparsity/clutter and occlusion/separability constraints that are not explained by visibility measures.

Collectively, these descriptors allow separation of domains that are visually degraded but structurally sparse from domains that are visually clean but crowded, supporting the controlled cross-domain analysis in subsequent sections. Due to page limitations, all metrics are detailed in Appendix A.

4 Experimental Design for Cross-Domain Analysis

Using the unified pipeline, we hold the detection architecture fixed and vary the *deployment domain* to quantify when extracted information remains comparable across environments. The design is structured to (i) select a stable, deployment-relevant detector, (ii) minimise confounding from suboptimal training, (iii) verify runtime feasibility on low-cost edge hardware, and (iv) test competing explanations for transfer failure: *visual degradation* versus *scene structure* using controlled stress tests grounded in the diagnostic metrics [Hendrycks and Dietterich, 2019]. Unless noted otherwise, we report standard detection metrics (mAP, precision, recall) to characterise both accuracy and failure asymmetries relevant to monitoring.

4.1 Detection Model Selection

We benchmark four YOLO variants under identical training conditions to select a baseline that is both (a) stable for controlled cross-domain analysis and (b) feasible under field deployment constraints. The evaluated models are YOLOv8m [Varghese and Sambath, 2024; Li *et al.*, 2025; Mohankumar and Anbalagan, 2025] and YOLO11n/YOLO11s/YOLO11m [Khanam and Hussain, 2024]. Each model is trained with the same schedule and evaluated on the Roboflow Aquarium baseline [Dwyer, 2022], with results reported in Table 2.

We select **YOLO11m** as the baseline [Liu *et al.*, 2025; Vijayalakshmi and Sasithradevi, 2025; Wilson *et al.*, 2025]. The selection is motivated by output stability under repeated runs, its practical compute/memory profile relative to larger

variants that are unlikely to fit common edge devices, and reduced deprecation risk given its recent release, as older architectures may lose framework support over the multi-year deployment timeline. We additionally follow Ultralytics guidance that prioritises YOLO11 for predictable memory usage and stable training behaviour in deployment-oriented settings [Ultralytics, 2025]. Importantly, the goal of this step is not to claim state-of-the-art accuracy, but to anchor subsequent cross-domain analyses on a single, reproducible detector.

4.2 Training and Optimisation Protocol

To ensure that observed performance differences are attributable to domain shift rather than training instability, YOLO11m is trained with a fixed, *pre-specified* optimisation protocol. Hyperparameters are selected via Bayesian optimisation using Optuna [Akiba *et al.*, 2019], motivated by sample-efficient search in high-dimensional spaces [Li *et al.*, 2022; Yu and Zhu, 2020]. Optimisation proceeds in two phases:

Phase 1: Core training parameters. We optimised the choice of optimiser and learning-rate schedule, regularisation parameters (e.g., dropout), and loss weights, with particular emphasis on bounding-box localisation to support small-object detection.

Phase 2: Augmentation parameters. With the core configuration fixed, we optimise augmentation strength [Liu *et al.*, 2024]. The final policy uses strong mosaic augmentation to increase exposure to occlusions and multi-object scenes, while limiting aggressive colour transformations. This constraint is deliberate: excessive colour jitter can inflate false positives in empty-water frames, which is operationally undesirable in monitoring settings where spurious detections can distort abundance indices and trigger unnecessary reviews.

4.3 Operational Feasibility: Edge Deployment Benchmarking

Because monitoring deployments often operate under limited power, memory, and connectivity, we evaluate whether the selected detector can sustain near-continuous inference on low-cost edge hardware. We target the NVIDIA Jetson Nano (4GB), representative of field-deployable nodes in remote or resource-limited settings. We measure inference latency (ms) and throughput (FPS) under three deployment formats: i) PyTorch (native): development baseline; ii) TorchScript: portable serialisation for embedded inference; and iii) TensorRT (FP16): hardware-optimised inference with kernel fusion and reduced precision. This protocol quantifies the performance gap between research execution and field constraints, and supports later discussion of economically scalable monitoring configurations.

4.4 Cross-Domain Evaluation Setup

We evaluate transfer reliability using two complementary components.

Unseen-domain evaluation. The trained model is applied to external datasets not used during training or optimisation to probe behaviour beyond the training distribution. The Fish

Video Object Tracking dataset [TrainingDataPro, 2022] contains synthetic underwater scenes with stylised textures and comparatively uniform backgrounds, while the Kaggle Fish Detection dataset [Larjeck, 2020] contains dense aquaculture footage with frequent occlusion and high object density. These datasets provide additional evidence that performance changes are not artefacts of the unified split construction.

Controlled stress tests informed by diagnostic metrics. To explicitly test whether cross-domain performance loss is driven primarily by *visual degradation* or by *scene structure*, we compute the diagnostic metrics of Section 3.4 across all domains and construct two targeted test splits. Each split isolates a distinct failure hypothesis while holding the detector fixed:

- **Scenario 1 (DeepFish): Visual degradation with structural sparsity.** The test split contains only **DeepFish** [Saleh *et al.*, 2020], a visually degraded domain (strong blur, low contrast) that is also structurally sparse (low object density and limited contextual redundancy). This scenario probes whether poor visibility alone explains transfer failure, or whether sparse structure causes disproportionate degradation even when targets are visually discernible.
- **Scenario 2 (Luderick): Habitat/colour shift with dynamic structure.** The test split contains only **Luderick** [Global Wetlands Project, 2020], which is comparatively cleaner in visibility but exhibits a strong habitat and colour shift (green seagrass background) and dynamic backgrounds. This scenario probes sensitivity to background semantics and structural dynamics under relatively favourable visual quality.

Together, these stress tests link performance variation to measurable domain properties (visual quality and structure metrics) rather than to architectural changes. This allows to attribute observed failures to specific, operationally interpretable drivers (e.g., sparsity versus turbidity; occlusion versus colour cast), supporting stakeholder-facing conclusions about when automated outputs can be treated as comparable monitoring evidence [Hendrycks and Dietterich, 2019].

5 Results

We evaluate the unified pipeline along three axes required for monitoring-grade information extraction: (i) baseline detection performance and model stability, (ii) transfer reliability under domain shift, and (iii) operational feasibility on low-cost edge hardware.

5.1 Baseline Model Selection

Table 2 compares four YOLO variants trained under identical conditions on the Roboflow Aquarium baseline. YOLOv8m achieves the strongest overall performance in mAP50–95, recall, and F1-score, while YOLO11m yields the highest precision and mAP50 with competitive overall accuracy.

For monitoring, precision is a critical guardrail against false positives that can bias downstream abundance indicators and inflate manual review effort. Together with its stable training behaviour and predictable memory profile in deployment-oriented settings, these considerations motivate

selecting YOLO11m as the fixed baseline for subsequent analyses.

Model	Params (M)	mAP50–95	mAP50	Precision	Recall	F1
YOLOv8m	25.9	0.4846	0.7901	0.7837	0.7356	0.7589
YOLO11n	2.6	0.3595	0.6977	0.7255	0.6102	0.6629
YOLO11s	9.4	0.4703	0.7499	0.7763	0.6588	0.7127
YOLO11m	20.1	0.4657	0.8097	0.8117	0.6866	0.7439

Table 2: Comparison of YOLO models on the Roboflow Aquarium dataset. YOLO11m is selected for its superior precision.

5.2 In-Domain Optimisation and Resolution

YOLO11m was fine-tuned at two resolutions (640×640 and 1024×1024) to test whether higher resolution yields meaningful gains. Increasing resolution to 1024 pixels yielded negligible changes in mAP and F1 (Table 3). Therefore, the 640×640 configuration is retained as the operational baseline, preserving efficiency without sacrificing reliability.

Configuration	mAP50–95	mAP50	Precision	Recall	F1
Validation (640px)	0.624	0.918	0.910	0.867	0.889
Validation (1024px)	0.621	0.913	0.907	0.866	0.886
Test (640px)	0.615	0.917	0.912	0.866	0.888
Test (1024px)	0.612	0.912	0.911	0.858	0.884

Table 3: In-domain performance of YOLO11m. Higher resolution offers diminishing returns.

5.3 Generalisation to External Domains

To probe behaviour beyond the unified split, the model was evaluated on two external datasets (Table 4). Performance remains strong on synthetic scenes (high precision), indicating robustness to texture shifts. In contrast, performance degrades sharply on dense aquaculture footage, where frequent occlusion reduces separability (Recall 0.318). This motivates the controlled experiments below.

Dataset	Images	mAP50–95	Precision	Recall	F1
Synthetic (Tracking)	99	0.557	0.827	0.715	0.767
Aquaculture (Dense)	629	0.255	0.804	0.318	0.456

Table 4: Performance on external unseen datasets. High density drives failure more than synthetic texture shifts.

5.4 Controlled Cross-Domain Stress Tests

We conducted two leave-one-domain-out stress tests. DeepFish and Luderick were selected as target domains to represent distinct failure hypotheses (Table 5).

Scenario 1: Context Collapse (DeepFish)

When DeepFish is excluded, performance drops sharply (Table 6). Correlation analysis (Figure 3) reveals this is driven by structural sparsity, not visual quality. DeepFish scenes lack contextual redundancy (schooling, habitat complexity); without these cues, the detector struggles to verify isolated targets, leading to a collapse in recall.

Scenario 2: Semantic Shift (Luderick)

When Luderick is excluded, the performance drop is moderate (Table 7). Despite strong colour/habitat shifts, the model generalises better than in DeepFish, confirming that visual/semantic shifts are less destabilising than structural ones.

Dataset	Turbidity	Contrast	BlurVar	Blue	Green	Red	UIQM	UCIQE	FishCount	Overlap	Difficulty
OzFish	0.00	0.80	0.88	1.00	1.00	1.00	0.48	1.00	1.00	1.00	0.82
DeepFish	0.95	0.81	0.98	0.31	0.37	0.33	0.57	1.00	0.16	0.24	0.57
Luderick	0.32	0.64	0.75	0.49	0.99	0.71	0.29	1.00	0.10	0.13	0.54
AquaCoop	0.33	1.00	1.00	0.25	0.00	0.12	1.00	0.00	0.51	0.97	0.52

Table 5: Normalised distortion and structure metrics. DeepFish represents Visual Degradation; OzFish represents Structural Complexity.

Split	mAP50–95	Precision	Recall	F1
Validation	0.604	0.891	0.835	0.862
Test (DeepFish)	0.285	0.616	0.552	0.583

Table 6: Scenario 1: Testing on DeepFish. Recall drops due to sparsity.



Figure 2: Sample inference image from scenario 1 (DeepFish). Blue bounding boxes indicate predictions, while white boxes denote ground truth.

Attribution of Failure Drivers: Structure vs. Vision

To attribute failure drivers without relying on small-sample domain correlations, we stratify evaluation frames by (i) *object density* (fish per image; bins: 0, 1, 2–3, 4–7, ≥ 8) and (ii) *structural overlap* (mean max-IoU among ground-truth boxes). Within each stratum, we compute recall and compare trends against stratification by visual covariates (turbidity, blur).

Across domains, recall is lowest in the sparsest strata, and the largest recall gaps occur between low-density and higher-density bins, consistent with the “Context Collapse” failure mode. In contrast, stratification by visual degradation yields weaker and less consistent gradients, indicating that visibility alone is not the dominant determinant of transfer reliability.

5.5 Operational Feasibility: Edge Deployment

We benchmarked inference on an **NVIDIA Jetson Nano (4GB)**, representative of commodity low-cost field nodes ($< \$150$). Benchmarks were executed at 640×640 resolution with batch size 1 to reflect deployment latency constraints (Table 8).

Engineering constraints. Under these settings, TorchScript conversion for YOLO11m exceeded the 4GB memory budget (*OOM*). This failure mode, invisible on server-grade hardware, highlights the necessity of hardware-aware optimisation in field deployments.

Monitoring policy feasibility. TensorRT (FP16) yields **3.45 FPS**. While insufficient for high-frequency tracking, this throughput supports periodic sampling policies used to ap-

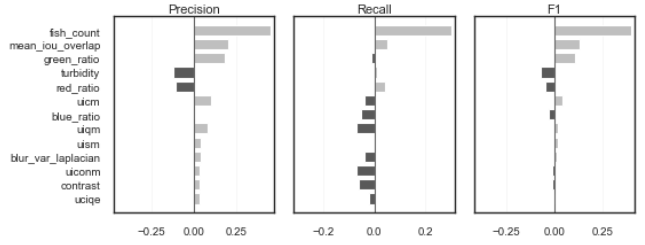


Figure 3: Horizontal Correlation Bars for Scenario 1. Performance tracks Structure (FishCount) more than Vision (Turbidity).

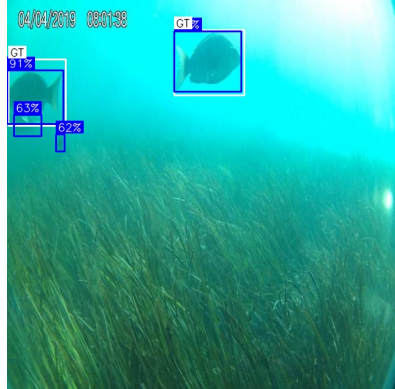


Figure 4: Sample inference image from scenario 2 (Luderick). Blue bounding boxes indicate predictions, while white boxes denote ground truth.

proximate frame-based abundance indices (e.g., *MaxN* computed over fixed time windows), enabling continuous low-rate sampling or burst-mode regimes that prioritise long-horizon coverage over per-second trajectory fidelity.

6 Discussion and Implications

This study reframes underwater fish detection from maximising in-domain benchmark scores to producing *monitoring-grade information* that remains comparable under domain shift and feasible under field constraints. Holding the detector fixed and varying deployment domains shows that transfer failures align more consistently with *scene structure* (sparsity, density, overlap) than with visual quality measures alone. Practically, this implies that improving visibility via enhancement is, by itself, an incomplete remedy: reliability depends on whether the scene provides sufficient contextual redundancy for verification and sufficient separability under occlusion.

Implications for monitoring protocols and data design. For practitioners, the actionable lever is *structural coverage*. Acquisition and curation should explicitly include (i) sparse

Split	mAP50–95	Precision	Recall	F1
Validation	0.608	0.899	0.850	0.874
Test (Luderick)	0.497	0.752	0.698	0.724

Table 7: Scenario 2: Testing on Luderick. Robustness is retained despite domain shift.

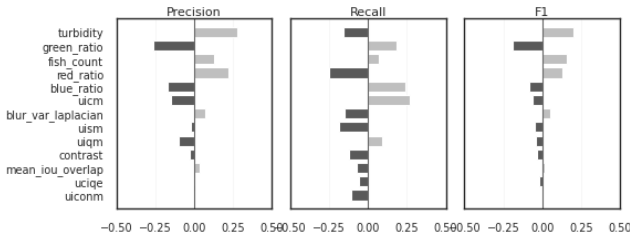


Figure 5: Horizontal Correlation Bars for Scenario 2.

regimes with isolated targets and (ii) crowded regimes with overlap/occlusion, rather than optimising only for clearer imagery. Reporting performance by interpretable strata (e.g., density and overlap bins) provides a deployment-facing reliability statement that is more portable than dataset names or single-number mAP summaries, and it supports cross-site comparability by linking expected error modes to observable site conditions.

Operational guardrails and reporting. Because false alerts impose review and bandwidth costs in low-prevalence deployments, precision should be treated as a guardrail and recall should be interpreted at operating points consistent with that guardrail (e.g., recall-at-fixed-precision). Under this framing, “reliability” is not a global property of the detector but a qualified claim conditional on structural regime (sparse versus crowded) and the operational threshold.

Edge feasibility and time-to-information. Edge benchmarking shows that deployment viability depends on the export/acceleration path. On 4GB-class nodes, naive serialisation may fail (OOM), whereas TensorRT enables practical throughput for periodic sampling policies. At 3.45 FPS, processing 1,000 frames is on the order of minutes (approximately 4.8 minutes), supporting long-horizon, low-rate monitoring without continuous uplink.

6.1 Limitations

Scope of claims. The analysis is intentionally architecture-controlled (a fixed detector) to support attribution under domain shift. Findings should be interpreted as evidence about *data- and environment-driven* reliability limits, not as a statement of detector state-of-the-art.

Binary detection abstraction. Collapsing taxonomy to a single `fish` class establishes a robust detection foundation but does not resolve species-level confusion, which is central for invasive-species decisions. Structure-driven failures may interact differently with fine-grained classification, particularly for rare taxa and small objects.

Frame-level evidence. The pipeline produces frame-level detections suitable for relative abundance proxies (e.g., MaxN-style indices) and alerting, but it does not recover

Model	Format	Latency	FPS	Gain
YOLO11n	PyTorch	111ms	8.99	–
YOLO11n	TensorRT	88ms	11.27	+25%
YOLO11m	PyTorch	450ms	2.22	–
YOLO11m	TorchScript		<i>Failed (OOM)</i>	
YOLO11m	TensorRT	290ms	3.45	+55%

Table 8: Edge inference on Jetson Nano. TensorRT makes Medium-sized models feasible for sampling.

identity-level continuity in dense shoals. Occlusion and group motion therefore remain constraints for behavioural inference and absolute counting.

Coverage of extreme regimes. Although the corpus is heterogeneous, extreme conditions (severe biofouling, near-blackout turbidity, very low-light) are underrepresented. Reliability in these regimes likely requires targeted data acquisition and human-in-the-loop fallback.

6.2 Future Work

Future work should (i) incorporate temporal consistency via lightweight tracking to mitigate transient misses, (ii) curate training data by *structural strata* (density/overlap) rather than dataset identity alone, (iii) add human-in-the-loop active learning that prioritises structurally out-of-distribution frames (especially sparse regimes associated with recall collapse), and (iv) evaluate tiered edge–cloud monitoring where the edge filters routine frames and transmits ambiguous cases for higher-capacity verification.

7 Conclusion

This work shows that reliable marine monitoring requires more than strong in-domain detection accuracy. By implementing a Unified Information Pipeline and evaluating a fixed detector under controlled cross-domain stress tests, we find that performance loss under transfer is explained more by *scene structure* (specifically, the “Context Collapse” phenomenon in sparse domains) than by visual degradation metrics alone. This challenges common assumption that image enhancement is the primary remedy for underwater AI [Awad *et al.*, 2024; Liu *et al.*, 2023], shifting emphasis toward structure-aware diagnostics as a prerequisite for comparable monitoring evidence.

Crucially, the pipeline is operationally grounded within an ongoing, multi-year European marine conservation initiative targeting invasive species management in Arctic and Atlantic waters. Edge benchmarking demonstrates that deployment-relevant inference is achievable on low-cost, resource-constrained hardware suitable for remote northern installations, supporting economically scalable monitoring in settings with limited connectivity. This foundational detection stage establishes reliability requirements for extending to species-level classification in operational deployments. Overall, the proposed system functions as an information-support tool: it standardises heterogeneous imagery, clarifies when automated outputs can be trusted across domains, and provides the technical foundation for experts to focus on the ecological interpretation required to protect marine biodiversity.

References

[AIMS *et al.*, 2019] AIMS, University of Western Australia (UWA), and Curtin University. Ozfish dataset — machine learning dataset for baited remote underwater video stations. <https://doi.org/10.25845/5e28f062c5097>, 2019. Accessed October 21, 2025.

[Akiba *et al.*, 2019] Takuya Akiba, Shotaro Sano, Toshihiko Yanase, Takeru Ohta, and Masanori Koyama. Optuna: A next-generation hyperparameter optimization framework, 2019.

[Awad *et al.*, 2024] Ali Awad, Ashraf Saleem, Sidiqe Paheding, Evan Lucas, Serein Al-Ratout, and Timothy C Havens. Beneath the surface: The role of underwater image enhancement in object detection. *arXiv preprint arXiv:2411.14626*, 2024.

[Bolya *et al.*, 2020] Daniel Bolya, Sean Foley, James Hays, and Judy Hoffman. Tide: A general toolbox for identifying object detection errors. In *European Conference on Computer Vision*, pages 558–573. Springer, 2020.

[Ditria *et al.*, 2020] Ellen M. Ditria, Sebastian Lopez-Marcano, Michael Sievers, Eric L. Jinks, Christopher J. Brown, and Rod M. Connolly. Automating the analysis of fish abundance using object detection: Optimizing animal ecology with deep learning. *Frontiers in Marine Science*, 7:429, 2020.

[Dwyer, 2022] Brad Dwyer. Aquarium combined dataset. <https://universe.roboflow.com/brad-dwyer/aquarium-combined>, 2022. Accessed October 21, 2025.

[Elmezain *et al.*, 2025] Mahmoud Elmezain, Lyes Saad Saoud, Atif Sultan, Mohamed Heshmat, Lakmal Seneviratne, and Irfan Hussain. Advancing underwater vision: a survey of deep learning models for underwater object recognition and tracking. *IEEE Access*, 2025.

[European Commission *et al.*, 2013] European Commission, Alterra, and Eurosita. Guidelines on climate change and *Natura 2000*: Dealing with the impact of climate change on the management of the *Natura 2000* network of areas of high biodiversity value. <https://data.europa.eu/doi/10.2779/29715>, 2013.

[European Commission, 2020] European Commission. Eu biodiversity strategy for 2030: Bringing nature back into our lives, 2020. Document 52020DC0380.

[Fisher *et al.*, 2016] Robert Fisher, Yun-Heh Chen-Burger, Daniela Giordano, Lynda Hardman, and Fang-Pang Lin, editors. *Fish4Knowledge: Collecting and Analyzing Massive Coral Reef Fish Video Data*, volume 104 of *Intelligent Systems Reference Library*. Springer International Publishing, 2016.

[Geirhos *et al.*, 2020] Robert Geirhos, Jörn-Henrik Jacobsen, Claudio Michaelis, Richard Zemel, Wieland Brendel, Matthias Bethge, and Felix A Wichmann. Shortcut learning in deep neural networks. *Nature Machine Intelligence*, 2(11):665–673, 2020.

[Global Wetlands Project, 2020] Global Wetlands Project. Luderick seagrass dataset. <https://github.com/globalwetlands/luderick-seagrass>, 2020. Accessed October 21, 2025.

[González-Sabbagh and Robles-Kelly, 2023] Salma González-Sabbagh and Antonio Robles-Kelly. A survey on underwater computer vision. *ACM Computing Surveys*, 55(13s):1–39, 2023.

[Han *et al.*, 2016] Song Han, Huizi Mao, and William J. Dally. Deep compression: Compressing deep neural network with pruning, trained quantization and huffman coding. In Yoshua Bengio and Yann LeCun, editors, *4th International Conference on Learning Representations, ICLR 2016, San Juan, Puerto Rico, May 2-4, 2016, Conference Track Proceedings*, 2016.

[Hendrycks and Dietterich, 2019] Dan Hendrycks and Thomas Dietterich. Benchmarking neural network robustness to common corruptions and perturbations. *Proceedings of the International Conference on Learning Representations*, 2019.

[Jian *et al.*, 2024] Muwei Jian, Nan Yang, Chen Tao, Huixiang Zhi, and Hanjiang Luo. Underwater object detection and datasets: a survey. *Intelligent Marine Technology and Systems*, 2(1):9, 2024.

[Joly *et al.*, 2015] Alexis Joly, Hervé Goeau, Hervé Glotin, Concetto Spampinato, Pierre Bonnet, Willem-Pier Vellinga, Robert Planquè, Andreas Rauber, Simone Palazzo, Robert Fisher, et al. Lifeclef 2015: Multimedia life species identification challenges, 2015.

[Khanam and Hussain, 2024] Rahima Khanam and Muhammad Hussain. Yolov11: An overview of the key architectural enhancements. *arXiv preprint arXiv:2410.17725*, 2024.

[Labrosse *et al.*, 2002] P. Labrosse, M. Kulbicki, and J. Ferrier. *Underwater Visual Fish Census Survey: Proper Use and Implementation*. Secretariat of the Pacific Community, Nouméa, New Caledonia, 2002. Accessed October 21, 2025.

[Larjeck, 2020] Larjeck. Fish detection dataset. <https://www.kaggle.com/datasets/larjeck/fish-detection-dataset>, 2020. Accessed: 2025-11-18.

[Li *et al.*, 2022] Zewen Li, Fan Liu, Wenjie Yang, Shouheng Peng, and Jun Zhou. A survey of convolutional neural networks: Analysis, applications, and prospects. *IEEE Transactions on Neural Networks and Learning Systems*, 33(12):6999–7019, 2022.

[Li *et al.*, 2025] Xingkun Li, Yuhao Zhao, Hu Su, Yugang Wang, and Guodong Chen. Efficient underwater object detection based on feature enhancement and attention detection head. *Scientific Reports*, 15(1):5973, 2025.

[Liu *et al.*, 2023] Hongmin Liu, Fan Jin, Hui Zeng, Huayan Pu, and Bin Fan. Image enhancement guided object detection in visually degraded scenes. *IEEE transactions on neural networks and learning systems*, 35(10):14164–14177, 2023.

[Liu *et al.*, 2024] Yingnan Liu, Yingtian Zou, Rui Qiao, Fusheng Liu, Mong Li Lee, and Wynne Hsu. Cross-domain feature augmentation for domain generalization. In *Proceedings of the Thirty-Third International Joint Conference on Artificial Intelligence, IJCAI '24*, 2024.

[Liu *et al.*, 2025] Mingxin Liu, Yujie Wu, Ruixin Li, and Cong Lin. Lfn-yolo: precision underwater small object detection via a lightweight reparameterized approach. *Frontiers in Marine Science*, 11:1513740, 2025.

[McGeady *et al.*, 2023] Ryan McGeady, Robert M Runya, James SG Dooley, John A Howe, Clive J Fox, Andrew J Wheeler, Gerard Summers, Alexander Callaway, Suzanne Beck, Louise S Brown, et al. A review of new and existing non-extractive techniques for monitoring marine protected areas. *Frontiers in Marine Science*, 10:1126301, 2023.

[Mieszkowska *et al.*, 2014] N. Mieszkowska, H. Sugden, L. B. Firth, and S. J. Hawkins. The role of sustained observations in tracking impacts of environmental change on marine biodiversity and ecosystems. *Philosophical Transactions of the Royal Society A*, 372:20130339, 2014.

[Mohankumar and Anbalagan, 2025] Vijayalakshmi Mohankumar and Sasithradevi Anbalagan. A benchmark dataset and ensemble yolo method for enhanced underwater fish detection. *ETRI Journal*, 2025.

[National Oceanic and Atmospheric Administration, 2025] National Oceanic and Atmospheric Administration. Invasive and exotic marine species. <https://www.fisheries.noaa.gov/insight/invasive-and-exotic-marine-species>, 2025. Accessed September 16, 2025.

[Panetta *et al.*, 2015] Karen Panetta, Chen Gao, and Sos Agaian. Human-visual-system-inspired underwater image quality measures. *IEEE Journal of Oceanic Engineering*, 41(3):541–551, 2015.

[Recht *et al.*, 2019] Benjamin Recht, Rebecca Roelofs, Ludwig Schmidt, and Vaishaal Shankar. Do imagenet classifiers generalize to imagenet? In *International conference on machine learning*, pages 5389–5400. PMLR, 2019.

[Roboflow, 2021] Roboflow. Fish 416x416 dataset. <https://public.roboflow.com/object-detection/fish>, 2021. Accessed October 21, 2025.

[Rourke *et al.*, 2022] Meaghan L Rourke, Ashley M Fowler, Julian M Hughes, Matt K Broadhurst, Joseph D DiBattista, Stewart Fielder, Jackson Wilkes Walburn, and Elise M Furlan. Environmental dna (edna) as a tool for assessing fish biomass: A review of approaches and future considerations for resource surveys. *Environmental DNA*, 4(1):9–33, 2022.

[Ruppert *et al.*, 2019] Krista M Ruppert, Richard J Kline, and Md Saydur Rahman. Past, present, and future perspectives of environmental dna (edna) metabarcoding: A systematic review in methods, monitoring, and applications of global edna. *Global Ecology and Conservation*, 17:e00547, 2019.

[Saleh *et al.*, 2020] Alzayat Saleh, Issam H. Laradji, Dmitry A. Konovalov, Michael Bradley, David Vazquez, and Marcus Sheaves. A realistic fish-habitat dataset to evaluate algorithms for underwater visual analysis. *Scientific Reports*, 10(1):14671, 2020.

[Torney *et al.*, 2019] Colin J. Torney, Dylan J. Lloyd-Jones, Maël Chevallier, David C. Moyer, Honest T. Maliti, Maternus Mwita, et al. A comparison of deep learning and citizen science techniques for counting wildlife in aerial survey images. *Methods in Ecology and Evolution*, 10(6):779–787, 2019.

[TrainingDataPro, 2022] TrainingDataPro. Fish tracking dataset. <https://www.kaggle.com/datasets/trainingdatapro/fish-tracking-dataset>, 2022. Accessed: 2025-11-18.

[Ultralytics, 2025] Ultralytics. Yolo twelve model overview. <https://docs.ultralytics.com/models/yolo12/#overview>, 2025. Accessed 07 December 2025.

[United Nations, 2015] United Nations. Transforming our world: the 2030 Agenda for Sustainable Development, Goal 14: Life Below Water, 2015. Accessed: 2026-01-19.

[Varghese and Sambath, 2024] Rejin Varghese and M Sambath. Yolov8: A novel object detection algorithm with enhanced performance and robustness. In *2024 International conference on advances in data engineering and intelligent computing systems (ADICS)*, pages 1–6. IEEE, 2024.

[Vijayalakshmi and Sasithradevi, 2025] M Vijayalakshmi and A Sasithradevi. Aquayolo: Advanced yolo-based fish detection for optimized aquaculture pond monitoring. *Scientific Reports*, 15(1):6151, 2025.

[Wang *et al.*, 2022] Jindong Wang, Cuiling Lan, Chang Liu, Yidong Ouyang, Tao Qin, Wang Lu, Yiqiang Chen, Wenjun Zeng, and Philip S Yu. Generalizing to unseen domains: A survey on domain generalization. *IEEE transactions on knowledge and data engineering*, 35(8):8052–8072, 2022.

[Wilson *et al.*, 2025] Katherine C Wilson, Moses Lurbur, and Noëlle Yochum. Automated fish detection in videos to support commercial fishing sustainability and innovation in the alaska walleye pollock (*gadus chalcogrammus*) trawl fishery. *ICES Journal of Marine Science*, 82(9):fsaf168, 2025.

[Xu *et al.*, 2023] Shubo Xu, Minghua Zhang, Wei Song, Haibin Mei, Qi He, and Antonio Liotta. A systematic review and analysis of deep learning-based underwater object detection. *Neurocomputing*, 527:204–232, 2023.

[Yang and Sowmya, 2015] M. Yang and A. Sowmya. An underwater color image quality evaluation metric. *IEEE Transactions on Image Processing*, 24(12):6062–6071, 2015.

[Yu and Zhu, 2020] Tong Yu and Hong Zhu. Hyperparameter optimization: A review of algorithms and applications, 2020.

A Metrics

A.1 Model Performance Metrics

Intersection over Union (IoU) measures the overlap between a predicted bounding box and its corresponding ground-truth annotation. It is the fundamental criterion behind all mAP computation. IoU is defined as:

$$\text{IoU} = \frac{|B_{\text{pred}} \cap B_{\text{gt}}|}{|B_{\text{pred}} \cup B_{\text{gt}}|}$$

mAP50 The mean Average Precision at IoU = 0.50 (mAP50) evaluates whether the model can correctly identify and localise fish under a relatively permissive bounding-box overlap requirement:

$$\text{mAP50} = \frac{1}{N} \sum_{i=1}^N \text{AP}_i(\text{IoU} = 0.50)$$

where AP_i denotes the Average Precision for class i . In this study, the task is binary (fish vs. background), so $N = 1$.

mAP50-95 The mean Average Precision computed across ten IoU thresholds from 0.50 to 0.95 in steps of 0.05, following the COCO evaluation protocol. This metric imposes increasingly strict localisation requirements and provides a more comprehensive view of the detector's performance:

$$\text{mAP50-95} = \frac{1}{10} \sum_{t=0.50}^{0.95} \text{AP}(\text{IoU} = t)$$

Precision Precision quantifies the proportion of predicted positive detections that are correct. High precision indicates that the model produces few false positives, which is important in underwater scenes where background clutter or floating particles may cause spurious detections:

$$\text{Precision} = \frac{TP}{TP + FP}$$

Recall Recall reflects how many true objects in the image received at least one correct bounding-box prediction. A high recall value indicates that the detector can capture most fish instances, even under challenging conditions such as turbidity, occlusion, low contrast, or motion blur:

$$\text{Recall} = \frac{TP}{TP + FN}$$

F1-Score The F1-score is the harmonic mean of Precision and Recall. This makes it particularly appropriate for underwater datasets, which often contain class imbalance:

$$\text{F1} = 2 \cdot \frac{\text{Precision} \cdot \text{Recall}}{\text{Precision} + \text{Recall}}$$

A.2 Image Degradation and Quality Metrics

Turbidity Turbidity estimates the level of haze caused by suspended particles in water. It is computed using a dark-channel prior proxy, where higher values indicate stronger scattering and reduced visibility:

$$\text{Turbidity} = \frac{1}{|\Omega|} \sum_{x \in \Omega} \min_{c \in \{r, g, b\}} I^c(x)$$

where Ω denotes the image domain and $I^c(x)$ is the intensity of colour channel c at pixel x .

RMS Contrast RMS contrast measures luminance variability in the image and reflects global visibility conditions:

$$\text{Contrast}_{\text{RMS}} = \sqrt{\frac{1}{|\Omega|} \sum_{x \in \Omega} (I_L(x) - \mu_L)^2}$$

Blur (Laplacian Variance) Image blur is estimated using the variance of the Laplacian operator, which captures edge strength:

$$\text{Blur}_{\text{var}} = \text{Var}(\nabla^2 I_L)$$

A.3 Colour Distribution Metrics

Red, Green, and Blue Ratios Colour ratios quantify channel dominance and underwater colour attenuation effects:

$$R_c = \frac{\sum_{x \in \Omega} I^c(x)}{\sum_{x \in \Omega} (I^r(x) + I^g(x) + I^b(x))}, \quad c \in \{r, g, b\}$$

with $R_r + R_g + R_b = 1$.

A.4 Underwater Image Quality Metrics

UIQM The Underwater Image Quality Measure (UIQM) combines colourfulness, sharpness, and contrast into a single score:

$$\text{UIQM} = c_1 \cdot \text{UICM} + c_2 \cdot \text{UISM} + c_3 \cdot \text{UIConM}$$

where $c_1 = 0.0282$, $c_2 = 0.2953$, and $c_3 = 3.5753$.

- **UICM** The Underwater Image Colourfulness Measure evaluates colour balance and distortion:

$$\text{UICM} = -\sqrt{\mu_{RG}^2 + \mu_{YB}^2} - 0.3\sqrt{\sigma_{RG}^2 + \sigma_{YB}^2}$$

where $RG = R - G$ and $YB = \frac{R+G}{2} - B$.

- **UISM** The Underwater Image Sharpness Measure quantifies edge strength using gradient magnitude:

$$\text{UISM} = \frac{1}{|\Omega|} \sum_{x \in \Omega} \sqrt{G_x(x)^2 + G_y(x)^2}$$

where G_x and G_y are Sobel gradients.

- **UIConM** The Underwater Image Contrast Measure evaluates local contrast using Michelson contrast over image blocks:

$$\text{UIConM} = \frac{1}{N} \sum_{i=1}^N \frac{I_{\max}^{(i)} - I_{\min}^{(i)}}{I_{\max}^{(i)} + I_{\min}^{(i)}}$$

UCIQE The Underwater Colour Image Quality Evaluation metric focuses on chroma dispersion, luminance contrast, and saturation:

$$\text{UCIQE} = \alpha \sigma_c + \beta \text{con}_L + \gamma \mu_s$$

with $\alpha = 0.4680$, $\beta = 0.2745$, and $\gamma = 0.2576$.

A.5 Scene Structure and Complexity Metrics

Fish Count Fish count measures scene density as the number of annotated objects in an image:

$$\text{FishCount} = |B|$$

where B is the set of ground-truth bounding boxes.

Mean Bounding Box Overlap Mean overlap quantifies occlusion severity using the average pairwise Intersection over Union between bounding boxes:

$$\text{MeanOverlap} = \frac{2}{N(N-1)} \sum_{i < j} \frac{|B_i \cap B_j|}{|B_i \cup B_j|}$$

where N is the number of bounding boxes in the image.

B Pipeline Schematic

This schematic provides a compact view of the full workflow: dataset aggregation and harmonisation, fixed-detector training with Optuna-tuned hyperparameters, external-domain checks, controlled stress tests, and edge optimisation/deployment.

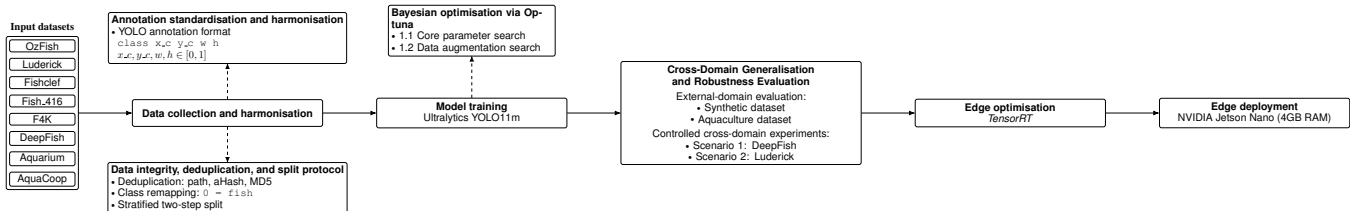


Figure 6: Pipeline from heterogeneous underwater datasets to a single-class fish detector (YOLO11m), including cross-domain evaluation and robustness analysis, and edge deployment on NVIDIA Jetson Nano.